ICARUS 30, 111–128 (1977)

A Calculation of Saturn's Gravitational Contraction History

JAMES B. POLLACK

Space Sciences Division, Ames Research Center, NASA, Moffett Field, California 94035

ALLEN S. GROSSMAN

Erwin W. Fick Observatory, Iowa State University, Ames, Iowa 50010 and Ames Research Center, NASA, Moffett Field, California 94035

RONALD MOORE

Erwin W. Fick Observatory, Iowa State University, Ames, Iowa 50010

AND

HAROLD C. GRABOSKE, JR.

Lawrence Livermore Laboratory, Livermore, California 94550

Received August 25, 1975; revised April 20, 1976

A calculation has been made of the gravitational contraction of a homogeneous, quasi-equilibrium Saturn model of solar composition. The calculations begin at a time when the planet's radius is ten times larger than its present size, and the subsequent gravitational contraction is followed for 4.5×10^9 years. For the first million years of evolution, the Saturn model contracts rapidly like a pre-main sequence star and has a much higher luminosity and effective temperature than at present. Later stages of contraction occur more slowly and are analogous to the cooling phase of a degenerate white dwarf star.

Examination of the interior structure of the models indicates the presence of a metallic hydrogen region near the center of the planet. Differences in the size of this region for Jupiter and Saturn may, in part, be responsible for Saturn having a weaker magnetic field. While the interior temperatures are much too high for the fluids in the molecular and metallic regions to become solids by the current epoch, the temperature in the outer portion of the metallic zone falls below Stevenson's [*Phys. Rev. J.* (1975)] phase separation curve for helium after 1.2 billion years of evolution. This would lead to a sinking of helium from the outer to the inner portion of the metallic region, as described by Salpeter [*Astrophys. J.* **181**, L83–L86 (1973)].

At the current epoch, the radius of the model is about 9% larger, while its excess luminosity is comparable to the observed value of Rieke [*Icarus* **26**, 37–44 (1975)], as refined by Wright [Harvard College Obs. Preprint No. 480 (1976)]. This behavior of the Saturn model may be compared to the good agreement with both Jupiter's observed radius and excess luminosity shown by an analogous model of Jupiter [Graboske *et al.*, *Astrophys. J.* **199**, 255–264 (1975)]. The discrepancy in radius of our Saturn model may be due to errors in the equations of state and/or our neglect of a rocky core. However, arguments are presented which indicate that helium separation may cause an expansion of the model and thus lead to an even bigger discrepancy in radius. Improvement in the radius may also foster a somewhat larger predicted luminosity. At least part and perhaps most of Saturn's excess luminosity is due to the loss of internal thermal energy that was built up during the early rapid contraction, with a minor contribution coming from Saturn's present rate of contraction. These two sources dominate Jupiter's excess luminosity. If helium separation makes an important contribution to Saturn's excess luminosity, then planetwide segregation is required.

Finally, because Saturn's early high luminosity was about an order of magnitude smaller than Jupiter's, water-ice satellites may have been able to form closer to Saturn than to Jupiter.

I. INTRODUCTION

Like Jupiter, Saturn radiates to space more energy than it absorbs from the Sun (Aumann *et al.*, 1969; Rieke, 1975). According to Rieke (1975), the ratio of these two quantities for Saturn equals 2.5 ± 0.6. In the case of Jupiter the excess energy is believed to have been derived directly or indirectly from gravitational energy release. All alternative energy sources, such as the decay of long-lived radioactive materials, fail by many orders of magnitude to supply the requisite energy (Graboske *et al.*, 1975b; Flasar, 1973; Hubbard and Smoluchowski, 1973). Since Saturn's internal energy source is only a factor of 10 weaker than that of Jupiter, a similar conclusion holds for Saturn.

As discussed by Flasar (1973), there are several classes of gravitational energy sources. We can distinguish the energy released in the absence of chemical differentiation from that made available due to differentiation. We can further subdivide the former into two subclasses that depend upon the sign of the change of the internal energy with time, $\dot{E}_{\rm INT}$. During the early phases of contraction when the fluid interior is easily compressible, the planet rapidly contracts and the change in the gravitational potential energy, $\dot{E}_{\rm GRAV}$, is large. At such times the release of gravitational potential energy both compensates for the excess energy radiated to space and leads to an increase in the internal energy, i.e., $\dot{E}_{\rm INT} > 0$. At later times, the interior becomes more incompressible, the planet contracts more slowly, and $\dot{E}_{\rm INT}$ becomes negative. In this case a significant part of the excess luminosity is supplied by the decay of the internal thermal reservoir. The ultimate origin of the internal energy reservoir is gravitational energy released at earlier epochs when the interior was more compressible.

Flasar (1973) has discussed an interesting limiting case for epochs characterized by $\dot{E}_{\rm INT} < 0$. During the latest stages of Jupiter's or Saturn's lifetime, the internal temperatures will be very low and consequently the thermal gas pressure, $P_{\rm T}$, due to ions, atoms, and molecules will be much less than the zero temperature pressure, P_0, due to the partially degenerate electrons, i.e., $P_{\rm T} \ll P_0$. In this limit, the luminosity is exactly balanced by the loss of the thermal component of the internal energy, $\dot{E}_{\rm INT}(T)$, and furthermore $\dot{E}_{\rm INT}(T) = \dot{E}_{\rm GRAV} = -\dot{E}_{\rm INT}\ (T = 0)$, where the last term is the time derivative of the zero temperature internal energy. Thus, the change in gravitational energy exactly compensates for the increase in the zero temperature internal energy and the excess luminosity is numerically equal in absolute value to both $\dot{E}_{\rm INT}(T)$ and $\dot{E}_{\rm GRAV}$. In the models of Saturn computed below, $P_{\rm T}$ cannot be neglected in comparison to P_0. For example, near the center of our Saturn model at the current epoch, $P_{\rm T} \approx 0.2\ P_0$ and larger ratios of $P_{\rm T}/P_0$ hold at earlier epochs. Consequently for our models it will make sense to say that, when $\dot{E}_{\rm INT} < 0$, part of the luminosity is derived from the decay of internal energy and part from the change in gravitational energy. At times later than our latest model, $P_{\rm T}$ will become much less than P_0 and Flasar's limiting case would be directly relevant.

So far we have discussed the gravitational energy sources that arise in the absence of chemical differentiation. Salpeter (1973) has suggested a model for the origin of Jupiter's current heat source that derives its energy from chemical differentiation. He suggested that when the temperatures became cool enough within the metallic hydrogen zone, helium would become partially immiscible in the metallic hydrogen and would begin to sink toward the planet's center. This mechanism could also be important for Saturn.

In summary, there are three major categories of gravitational energy sources: gravitational energy released by contraction in the absence of differentiation; the decay

of internal energy initially accumulated by prior contraction; and the energy released by chemical differentiation.

Grossman *et al.* (1972) and Graboske *et al.* (1975b) (hereafter referred to as Paper I) have investigated the source of Jupiter's internal energy by studying the temporal evolution of homogeneous, gravitationally contracting models. In Paper I, a good match was achieved between Jupiter's observed radius and that exhibited by the model after 4.5 billion years of evolution. However, the predicted excess luminosity was about a factor of 2 smaller than the observed value. As shown in Fig. 4 and discussed below, a new, better-determined value for Jupiter's excess luminosity is substantially lower than the value used in Paper I and as a result the predicted luminosity is now close to the observed value. Thus, a large fraction of Jupiter's present excess energy can be accounted for by the first two gravitational energy components above. This result limits the possible contribution arising from the chemical separation term for Jupiter. Of the first two components the energy from the thermal reservoir is the dominant term at the present epoch. However, the current rate of contraction makes an important, secondary contribution to the internal energy source.

According to the calculations in Paper I, Jupiter's excess luminosity was many orders of magnitude ($\lesssim 7$) higher during its early contraction history than at present. Pollack and Reynolds (1974) suggested that water-ice condensation was inhibited close to Jupiter during this early high-luminosity phase. As a result, the inner Galilean satellites were formed with a smaller proportion of water ice than the outer ones. This conclusion is consistent with the observed systematic variation of the Galilean satellites' mean density with distance from Jupiter.

In this paper we perform a set of calculations of Saturn's gravitational contraction history that is analogous to the one performed for Jupiter in Paper I. Thus, we study the evolution of a homogeneous Saturn that is composed of a solar abundance mixture of elements, and we do not allow for either the presence of a core composed of a rock–ice mixture, as has been suggested by Podolak and Cameron (1974), or the possible separation of helium from hydrogen. In view of the good match achieved by the homogeneous Jupiter model with the planet's observed radius and excess luminosity, it is important to perform such a comparison for an analogous model of Saturn. The results of our evolutionary calculations will provide estimates of the contribution of the first two modes of gravitational energy release to Saturn's observed excess luminosity and will permit an assessment of whether the interior has cooled sufficiently for helium to begin separating from metallic hydrogen. We will also briefly consider the implications of Saturn's early contraction phase for the formation of its satellite system and rings. However, this topic will be discussed more extensively in another paper (Pollack *et al.*, 1976). For all these problems, a comparison will be made between the behavior of Saturn and that of Jupiter. Finally, we will compare the internal structure of our current epoch, homogeneous model of Saturn with an inhomogeneous model containing a rocky core to assess the sensitivity of some of our conclusions to plausible perturbations.

II. COMPUTATIONAL METHOD

Our objective is to determine the evolution with time of a model Saturn. This leads to a specification of the temporal variation of such quantities as the planet's radius, central temperature, central density, and luminosity. In the next section, the observed values of radius and excess luminosity are compared with the corresponding quantities predicted by the model calculations after 4.5 billion years of evolution, the approximate age of the solar system, to assess the validity of the models. Below we briefly describe the basic method of calcu-

lation, the model atmospheres, the thermodynamic properties of the planetary material, and the choice of model parameters. We stress the underlying assumptions and limitations of the calculations. Our procedure is described in greater detail in Paper I.

The evolutionary calculations refer to an intermediate stage of Saturn's history, one that spans a large fraction of the time from the beginning of the solar system until today. Preceding the point at which our calculations begin is the stage in which Saturn was being formed. During this initial period Saturn's mass increased with time. In addition, due to the formation of extensive zones of ionization and dissociation inside the planet, Saturn underwent a hydrodynamical collapse during at least part of this phase (Perri and Cameron, 1974; Bodenheimer, 1974). At the end of this stage Saturn achieved a quasi-hydrostatic equilibrium configuration at a size much larger than its present dimension. Calculations by Bodenheimer (1974) indicate that Jupiter ceased collapsing hydrodynamically at a radius that is four to five times larger than its present value. A similar value may hold for Saturn. Our calculations begin at a radius ten times larger than the current value. Subsequent contraction apparently occurs slowly enough that at each point in time the model can be assumed to be in hydrostatic equilibrium. The relationship between one model and the subsequent one is dictated by the amount of excess energy radiated to space during the time interval separating the two models. The stage of evolution studied in our calculations is succeeded by a stage characterized by the separation of helium from hydrogen. This period commences when the interior temperatures fall below the critical temperature for H/He immiscibility.

Several basic assumptions or limitations enter into our calculations. The models are chemically homogeneous, nonrotating, and therefore spherically symmetric, and completely convective. The first assumption has been discussed in the Introduction and will be considered in subsequent sections. The neglect of rotation is unimportant for our purposes. According to Kieffer (1967) our computed radius will be about 2% too small as a result of this assumption. Finally, some justification for the assumption of convective energy transport in the interior is given by the temperature structure computed for our model atmospheres (see below) and Hubbard's (1968) examination of the opacity present in the deep interior of Jupiter. Because convection is a very efficient mode of energy transport at the densities and luminosities of interest (Hubbard, 1968; Pollack and Ohring, 1973), the assumption of convective transport implies an adiabatic relationship between temperature, pressure, and density.

As described in more detail by Paper I, the interiors of the models are calculated by the Henyey method (Kippenhahn *et al.*, 1967). This method is an iterative technique for determining the structure of each successive model so as to satisfy the equations of mass conservation, hydrostatic equilibrium, energy transport, and energy conservation. The last of these equations involves a time derivative that links the current model of interest with prior models. We arbitrarily take as our initial model one having a radius that is ten time larger than Saturn's present size, 10 R_S. The evolutionary tracks very quickly become insensitive to the choice of initial conditions. For example, in the evolutionary calculations for Jupiter, the maximum value of the central temperature changed by less than 1% when the starting radius was changed from $16R_J$ to 3.5 R_J, where R_J is Jupiter's present radius.

To specify one of the outer boundary conditions for the interior models, it was necessary to calculate a grid of model atmospheres. The method of Pollack and Ohring (1973) was used to determine a temperature structure near the top of the atmosphere that was consistent with a

specified net flux. Allowance was made for opacity due to molecular hydrogen, water vapor, ammonia, and methane. We assumed that the solar insolation flux was deposited entirely at the bottom of the model atmosphere. Thus, the specified net flux of a given model atmosphere consisted of the sum of the internal flux and the solar insolation flux. If we quantify these fluxes in terms of an effective temperature, then the total effective temperature T_{es} is related to the effective temperatures of the insolation and internal fluxes $T_{e\odot}$ and $(T_e)_{int}$, respectively, by

$$T_{es}^4 = T_{e\odot}^4 + (T_e)_{int}^4. \quad (1)$$

For the present epoch, T_{es} is the quantity that is found from Saturn's measured thermal emission, and $T_{e\odot}$ is determined from Saturn's reflectivity spectrum.

Model atmospheres were calculated at a grid of values of surface gravity (and hence planetary size) and total effective temperature. All model atmospheres were found to have a convection zone which was present in the higher pressure portions of the atmospheres. The object of these calculations was a specification of a temperature–pressure point near the top of the convection zone for each model atmosphere. The model atmospheres are unrealistic in the stratospheric regions because of the assumption made about the solar energy deposition. However, they provide quite good estimates of the desired temperature–pressure point. For example, Pollack and Ohring's (1973) determination of this point at the top of the convection zone for current-day Jupiter is in excellent agreement with the point determined empirically by Houck *et al.* (1975) from their infrared spectral observations of Jupiter.

The calculation of thermodynamic properties of the planetary material has been discussed by Graboske *et al.* (1975a). The properties calculated as functions of temperature and density are pressure and enthalpy, their derivatives, and such second-order thermal properties as the adiabatic gradient, specific heat at constant pressure, and $(\partial \ln \rho/\partial \ln T)_P$, where ρ, T, and P are density, temperature, and pressure, respectively. These quantities were calculated for densities ranging from 10^{-7} to 10 g cm^{-3} and for temperatures ranging from 60 to 60 000°K. The mixture used in these calculations consisted of the following atoms, molecules, and ions: H_2, H_2^+, H^-, H, H^+, He, C, N, and O, and the ions of the last four species.

The low-density ($\rho \lesssim 0.1$ g cm^{-3}) equation of state (EOS) was calculated by a free-energy minimization method which included such nonideal interactions as perturbation of ground-state energies of atoms and molecules by their neighbors, coulomb interactions, and interatomic interactions. The high-density EOS calculations ($\rho \gtrsim 1$ g cm^{-3}) were made using a modified Thomas–Fermi method. Thermodynamic properties in the intermediate-density regime were obtained by smoothly interpolating values obtained at higher and lower densities, while ensuring that certain basic thermodynamic relationships were satisfied. Needless to say, the thermodynamic quantities of interest are least known in this intermediate-density region, where errors up to several tens of percent may occur for some of the second-order quantities.

The calculations were performed for the same solar abundance mixture of elements as that used in Paper I for Jupiter. The mass fraction of hydrogen, helium, and other elements, as well as the observed or inferred properties of present-day Saturn, are summarized in Table I.

III. RESULTS

The results of the evolution calculations are presented in Figs. 1 to 9 and Table II.

In Fig. 1 we show the path of the evolving model in the Hertzsprung–Russell (H–R) diagram. The coordinates of the diagram are the internal luminosity $L_{int}/L_\odot$ expressed in solar luminosity units, and the internal

TABLE I

Properties of Saturn Used for the Calculations of This Paper

Property	Symbol	Comment	Value
Mass[a]	$M/M_\odot$	Observed	0.000286 solar masses
Mean radius[a,b]	R_s	Observed	5.779×10^9 cm
Mean density[a]		Observed	0.704 g cm^{-3}
Total effective temperature	T_{es}	Observed	95.6 ± 5°K[c] (85 ± 2°K)[d]
Insolation effective temperature[c]	$T_{e\odot}$	Observed	76 ± 4°K
Internal luminosity[e]	$\log (L_{int}/L_\odot)$	Observed	-9.515 ± 0.2
Ratio of thermal energy emission to solar energy absorption	—	Observed	2.5 ± 0.6[c] ($1.44^{+0.44}_{-0.20}$)[d]
Age	t_s	Inferred[e]	4.5×10^9 years
Chemical composition[f]:			
Mass fraction of H	X	Based on solar abundances	0.74
Mass fraction of He	Y		0.24
Mass fraction of other elements	Z		0.02

[a] From Newburn and Gulkis (1973).
[b] Volumetric average.
[c] From Rieke (1975).
[d] From Wright (1976), based on a recalibration of Mars' brightness temperature.
[e] Based on the age of the solar system.
[f] See Paper I.

effective temperature $(T_e)_{int}$. (The term "internal" refers to the energy flux derived from the deep interior of the planet and thus excludes that portion of the energy flux derived from the solar energy deposition. Internal energy and excess energy are equivalent terms.) The circle with an adjacent S indicates the observed position of Saturn in this figure, with the size of the surrounding rectangle indicating the uncertainty in this position. Numbers associated with crosses indicate the evolution time from the start of the calculation. During the early part of the track, the model evolves approximately vertically in the H–R diagram; i.e., the effective temperature remains almost constant while the luminosity steadily decreases. This portion of the evolutionary path closely resembles the pre-main sequence track of stars in the mass range of 0.1 to 0.3 solar masses (Grossman and Graboske, 1971). During the initial contraction phase, the value of T_{es}, which is due almost entirely to the internal component of luminosity, is of the order of 600°K, a value much higher than the present value of 95°K. The cosmogonic implications of this early stage of high luminosity and high effective temperature will be discussed briefly in the next section. At approximately 10^6 years, when the radius is close to 2 R_s, the evolutionary track changes character and approaches that of a cooling white dwarf star. Note that the evolutionary track passes quite close to the present location of Saturn in the diagram. However, passage by Saturn's position occurs at approximately 2×10^9 years rather than 4.5×10^9 years. More will be said on this matter below.

Further insight into the two phases of the evolutionary track is provided by Fig. 2, which shows the variation of central temperature T_c with central density ρ_c. Time tick marks are also shown on the evolutionary track. As was the case for Jupiter, the

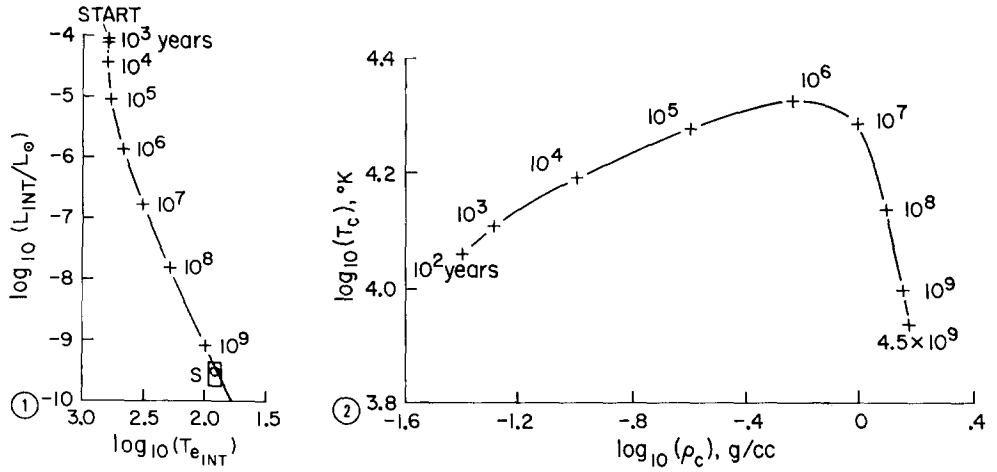

FIG. 1. Hertzberg–Russell diagram of $L_{int}/L_\odot$ as a function of $(T_e)_{int}$ for a Saturn contraction sequence with $T_{e\odot} = 76°K$, where $L_{int}/L_\odot$, $(T_e)_{int}$, and $T_{e\odot}$ are the ratio of the internal luminosity to the solar value, the internal effective temperature, and the insolation effective temperature, respectively. Values of time from the start of the calculation are shown by the numbers next to crosses along the evolutionary track. The observed values of present-day Saturn are shown by the circle enclosed by rectangle. The size of the rectangle provides a measure of the uncertainty in the observed values.

FIG. 2. Central temperature T_c as a function of central density ρ_c for the Saturn contraction sequence. The numbers next to crosses along the evolutionary track indicate the time from the start of the calculation.

value of T_c increases during contraction as long as the free electron gas behaves as an ideal Maxwell–Boltzmann gas. However, after about 10^6 years of evolution, electron degeneracy sets in near the center of the planet. These regions undergo very little subsequent contraction, and begin to cool. With the passage of time, the zone of partial degeneracy spreads outward from the center of the model. The point in the evolutionary track where the model reaches a maximum value of T_c is a convenient line of demarcation between the pre-main sequence and white dwarf cooling phases. The maximum value of T_c is about 21 000°K, and it is achieved after about 10^6 years of evolution when the radius is about 2 R_s. As in the case of Jupiter, this peak value of T_c is far below the value required for the onset of nuclear burning of deuterium, the isotope with the lowest ignition point. Thus, the giant planets have no main sequence stage of evolution. In this regard they differ significantly from their more massive stellar counterparts.

In Fig. 3 we examine the time variation

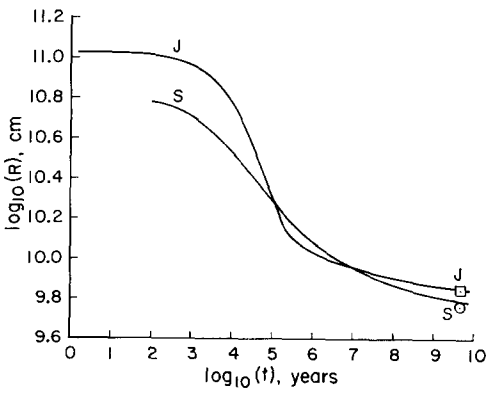

FIG. 3. Radius R of Saturn and Jupiter as a function of time t. The evolutionary track for Jupiter was obtained from the calculations of Paper I. The observed values of the radius at the 4.5×10^9-year time point are indicated by the square with a J for Jupiter and the circle with an S for Saturn. These observed values have negligible error bars.

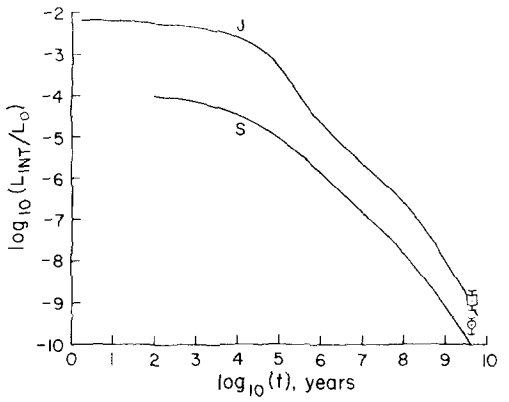

FIG. 4. Internal luminosity in solar units $L_{int}/L_\odot$ of Saturn and Jupiter as a function of time t. The evolutionary track for Jupiter was obtained from the calculations of Paper I. Also shown by the square and associated J and the circle and associated S are the observed values for Jupiter and Saturn, respectively, at the 4.5×10^9-year time point. The vertical lines attached to the observed values show the quoted error bars.

of the radius R of Saturn. The corresponding evolutionary track for Jupiter is also shown. The square flanked by the letter J and the circle flanked by the letter S indicate the observed values of radius for Jupiter and Saturn, respectively, at a time of 4.5×10^9 years. Contraction of the Saturn model from an initial radius of 10 R_s to 2 R_s is condensed into the first million years of evolution. Almost the whole lifetime of the planet is spent in the collapse from $2R_s$ to its present radius. As explained above, this behavior is due to the onset of electron degeneracy effects at about 2 R_s, which inhibit large-scale contraction. Thus, the planet is forced into a state of thermal cooling at practically constant radius. Jupiter shows a similar type of behavior, although degeneracy sets in at a somewhat earlier time ($\sim 10^5$ years) than for Saturn.

The evolutionary track for Jupiter passes almost exactly through the observed radius. However, the track for Saturn has a value at 4.5×10^9 years, which is about 9% larger than its measured radius. We discuss this matter further in the next section.

The time tracks of Saturn's and Jupiter's internal luminosity L_{int} are shown in Fig. 4. The observed values with their associated error bars at a time of 4.5×10^9 years are indicated by the square and associated J, and the circle and associated S for Jupiter and Saturn, respectively. Several remarks need to be made about the observed values used for this figure. The value shown for Jupiter was derived from the observations by the Pioneer 10 and 11 infrared radiometers (Ingersoll *et al.*, 1975). Because this experiment was well calibrated, its result supplants the older determination of Jupiter's excess luminosity by Aumann *et al.* (1969), who first discovered this important effect. The observed data point for Saturn was adopted from the work of Rieke (1975), who carefully separated the thermal emission of the rings and planet.

The calculated evolutionary track of Jupiter's internal luminosity passes very close to the observed value at a time equal to the age of the solar system. This result supercedes that of Paper I, where these investigators were unable to match the value given by their nominal model with the observed value of Aumann *et al.* (1969). A still further revision of the infrared luminosity of Jupiter has been suggested by Orton and Aumann (1976). Their ground-based observations of Jupiter in the 12 to 25 μm spectral region yield fluxes that are about 20% smaller than those that would have been expected on the basis of the Pioneer infrared radiometer data. The cause for this discrepancy is under investigation. A 20% decrease in Jupiter's *total* infrared luminosity would result in an even better agreement between the observed and predicted *excess* luminosities.

According to Fig. 4, the internal luminosity of Saturn at 4.5×10^9 years is a factor of 3 smaller than the observed value. Note that the calculated luminosity at the 2×10^9 year point is comparable to the currently observed value. However, a study by Wright (1976) suggests a significant reduc-

tion in the observed excess of Saturn. In deriving the total infrared luminosity of Saturn, Rieke (1975) combined well-calibrated observations of Saturn and its rings at wavelengths shortward of 30 μm with aircraft observations at longer wavelengths. The latter were calibrated by assuming that Mars had a brightness temperature of 240°K. Wright (1976) points out that the brightness temperature of Mars varies with orbital position and phase angle. His model calculations indicate that a lower brightness temperature for Mars would have applied at the time of the aircraft observations and consequently the excess luminosity of Saturn may be as much as a factor of 3 smaller than the value estimated by Rieke and shown in Fig. 4. Such a reduction would lead to a substantial improvement in the agreement between the observed and predicted excess luminosities. The precise value of the excess luminosity implied by the recalibration of Mars is under current investigation.

In Fig. 5 we study the energy changes that take place during Saturn's evolution. The curves marked "GRAV" and "INT" show the value of $(-E_{\mathrm{GRAV}})$ and (E_{INT}), respectively, as a function of time, t. E_{GRAV} and E_{INT} are the gravitational potential energy and the internal thermal energy, respectively. The initial contraction leads to a rapid change in the gravitational energy, which permits the internal thermal energy to increase, despite the large amount of radiation emitted to space. As the contraction slows down after about 10^6 years of evolution, the gravitational energy release is too small to meet the luminosity requirements. In order to balance the energy budget, the interior cools. At present most of the internal luminosity of Fig. 4 for Saturn is supplied by the decrease in the internal thermal energy. However, the change in the gravitational energy at the current epoch is still significant, and it makes a nonnegligible secondary contribution to the observed excess luminosity. A similar situation holds for Jupiter.

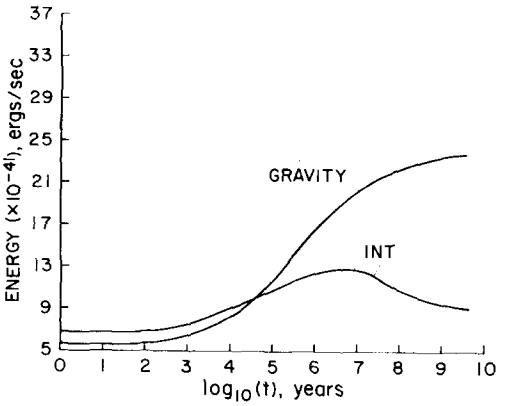

FIG. 5. Variation with time t of $(-E_{\mathrm{GRAV}})$, labeled GRAV, and (E_{INT}), labeled INT, for the Saturn contraction sequence, where E_{GRAV} and E_{INT} are the gravitational potential energy and internal thermal energy, respectively.

Table II summarizes a number of key parameters of selected models in the contraction sequence. These models include the initial model (model 1), the model having the maximum value of the central temperature $(T_c)_{\max}$ (model 2), models close to the time points of 2×10^9 (model 3) and 4×10^9 years (model 4), and finally the model for the current epoch (model 5). Model 5 is characterized by a central temperature of about 7300°K and a central density of about 1.46 g cm^{-3}.

We next discuss the internal structure of our evolutionary models in greater detail. Figure 6 shows the temperature–density structures of models 1, 2, and 3. The corresponding curves for models 4 and 5 lie slightly below the curve of model 3. The low-density end point of each model refers to a point near the top of the convection zone, i.e., near optical depth unity in the planetary photosphere, while the high-density end point refers to the center of the model. The short, vertical line transecting each curve denotes a point, interior to which 97% of the planetary mass resides. This figure illustrates the transition from the ex-

TABLE II

Parameters of Models in the Saturn Contraction Sequence

Model	Age (years)	$(T_e)_{int}$[a] (°K)	Internal luminosity, in solar units	Radius in units of observed value	Central density (g cm^{-3})	Central pressure (dynes/cm^2)	Central temperature (°K)
1. Initial model	0	611	9.86×10^{-5}	10.69	3.89×10^{-2}	2.40×10^{10}	11350
2. At $(T_c)_{max}$	1.22×10^{6}	447	1.04×10^{-6}	2.06	6.34×10^{-1}	1.288×10^{12}	21330
3.	1.95×10^{9}	81	3.24×10^{-10}	1.102	1.426	4.365×10^{12}	8220
4.	3.98×10^{9}	62	1.08×10^{-10}	1.089	1.455	4.467×10^{12}	7460
5. Present epoch	4.5×10^{9}	58	8.47×10^{-11}	1.087	1.459	4.467×10^{12}	7310

[a] Internal effective temperature.

tended core of model 1 to the compacted dense core of model 3. The peak central temperature of model 2 is much lower than the corresponding value for Jupiter, while its central density is much higher. As a result the highly ionized phase exhibited by Jupiter in its early history is not mimicked by Saturn.

For most of Saturn's evolutionary history, the central density and pressure increase, while its central temperature decreases. Thus, it is important to inquire about the phase changes that accompany these variations. There are three phase changes of particular interest. These are the change from a molecular fluid to a metallic fluid, the crossing of the immiscibility gap of helium in metallic hydrogen, and the transition from a fluid phase to a solid phase. Below, we address each of these possibilities. However, the conclusions drawn for Saturn are more tentative than those for Jupiter as a result of several factors. First, the fit of the current-day homogeneous model for Jupiter to the observed radius is much better than that for Saturn. Second, and perhaps relevant also to the first point, a larger fraction of Saturn's mass lies within a region of the dense molecular fluid ($0.1 \lesssim \rho \lesssim 1$ g cm^{-3}) for which the EOS is least known. As discussed in the Introduction, the EOS used in our calculations should be fairly accurate outside of this region.

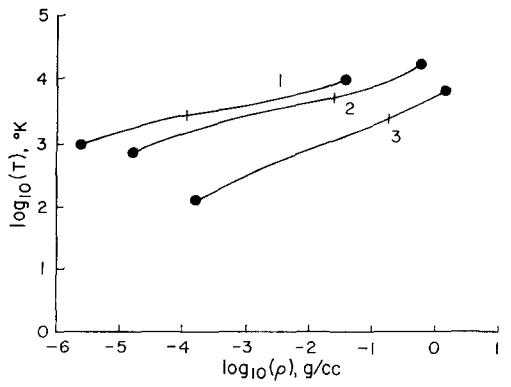

FIG. 6. Temperature–density (T–ρ) structure of models 1, 2, and 3. The low-density end point for each curve corresponds to a point close to the photosphere, while the high-density end point is the center of the planet. The short vertical line denotes the point interior to which 97% of the planetary mass lies.

When the central pressure rises to a large enough value, molecular hydrogen undergoes a phase transition to metallic hydrogen. The point at which this occurs is a subject of considerable debate. Recent experimental results purporting to have observed this transition are apparently not reliable (Ross *et al.*, 1975), while theoretical

predictions cover a wide range. The best current value for pressure at this transition is 3 mbar (Ross, 1974; Ross *et al.*, 1975). Using this value, we find that the metallic region for Paper I's model of current-day Jupiter extends to $M_r/M_J = 0.77$ at $r/R_J = 0.78$, where M_r, M_J, r, and R_J are the mass interior to radius, r, the mass of Jupiter, radial distance, and the radius of Jupiter, respectively. This result is consistent with the findings of earlier studies (Hubbard and Smoluchowski, 1973). For Saturn, the calculations of this paper indicate the presence of a much smaller metallic hydrogen core. At the current epoch, $M_r/M_s = 0.125$ at $r/R_s = 0.37$. Because of the limitations of our models, these values for Saturn should be considered as very tentative. On the one hand, the fact that the current epoch model has a radius that is about 9% larger than the observed value implies that the actual central pressure and hence the zone of metallic hydrogen will be larger than they are for this model. On the other hand, the presence of a small rocky core at the center of Saturn, as advocated by Podalak and Cameron (1974), would mean that this zone would be smaller.

The evolutionary track for the central density and pressure is illustrated in Fig. 7. We see that the central pressure reaches a value of 3 mbar after about 3×10^7 years of evolution. At this point the metallic zone begins to form and its size continually increases with time. In the next section we discuss the implications of a small metallic core for the generation of a magnetic field.

Next, is it possible that the interior of Saturn overlaps the H/He immiscibility gap, with the resultant gravitational separation of a He-rich phase toward the planet's center? A detailed study of the thermodynamics of H/He *metallic* fluids has been carried out by Stevenson (1975). He found that atomic helium, treated as helium nuclei immersed in a proton fluid, became immiscible when the temperature fell below a critical value which increased somewhat

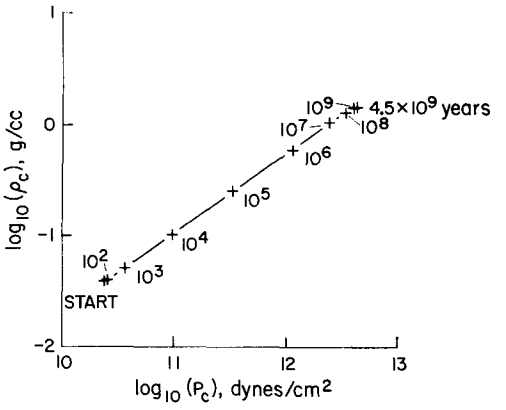

FIG. 7. Evolutionary track of the central density and pressure. The numbers next to crosses along the evolutionary track indicate the time from the start of the calculation.

with decreasing pressure. In Fig. 8 the H/He phase separation curve is shown for the solar composition used in our calculations. Also shown are the molecular/metallic phase boundary and the evolutionary tracks of our models at this latter boundary and the center of the planet. We see that the outer edge of the metallic zone transits the immiscibility boundary after about 1.2×10^9 years of evolution. However, the center of the planet does not cross the phase separation curve until almost 3×10^9 years later. As discussed more fully in the next section, the gravitational separation of helium from hydrogen in the metallic zone of Saturn should lead to an enhanced excess luminosity. According to the calculations in Paper I, the temperatures in the metallic zone of present-day Jupiter lie far above Stevenson's immiscibility boundary. Gravitational separation of He from H apparently does not occur for Jupiter until a later stage in its history.

Smoluchowski (1967) suggested that the interior of Jupiter might be cold enough to permit the formation of solid molecular hydrogen. Although this suggestion seems unlikely in view of the high temperatures and extensive metallic region exhibited by more recent models (Paper I; Hubbard and

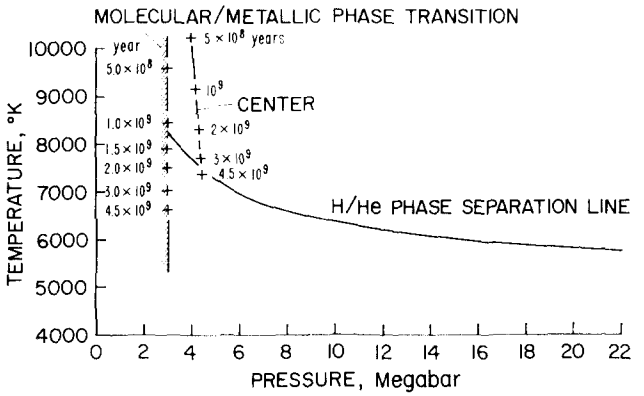

FIG. 8. Phase boundaries for the molecular and metallic phases of hydrogen and for the separation of helium from hydrogen. For points lying below the separation line, helium becomes partially immiscible in metallic hydrogen. This curve was derived from Stevenson's (1975) calculations for a solar abundance mixture of H and He. Also shown on the diagram is the evolutionary track of the center of Saturn. Numbers next to crosses on this track and on the molecular-metallic phase boundary indicate the time from the start of the calculations.

Smoluchowski, 1973), it perhaps has more relevance for the much cooler interior of Saturn. Figure 9 shows Ross' (1975) freezing curve for *pure* molecular hydrogen, as derived from a generalized Lindemann's melting law and the best semiempirical H_2 potential. Also shown is the interior structure of the molecular hydrogen region of our present-day Saturn model. We see that the molecular region of the current-day model lies about 3000°K above the freezing curve. Allowance for impurities (He) within the molecular hydrogen fluid will lead to a decrease in the freezing-point curve. It is extremely improbable that changes in future model sequences will alter the temperature structure to a position below the freezing curve. Therefore, solid H_2 can be ruled out for Saturn interiors. Similarly the temperatures are much too high for metallic hydrogen to freeze (Hubbard and Smoluchowski, 1973).

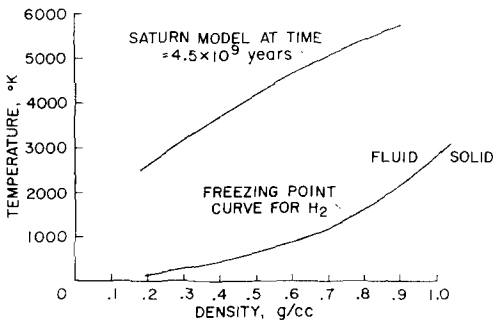

FIG. 9. A comparison between the temperature–density structure of the molecular hydrogen envelope for the 4.5 × 10^9-year-old model and the phase boundary between fluid and solid molecular hydrogen.

IV. DISCUSSION

In this section we discuss factors that may lead to a better fit between the radius and luminosity of the models and the observed values; we relate the value of Saturn's magnetic field strength to the interior structure of our models; we assess the effect of a silicate core on our conclusions; and finally, we briefly consider the effect of Saturn's early high-luminosity phase on the formation of its satellites and rings.

Fit to the Observed Radius

As illustrated in Fig. 3, the evolutionary track of a homogeneous Jupiter with a solar abundance of elements passes almost exactly through Jupiter's observed radius after 4.5 billion years, the approximate age

of the solar system. However, the Saturn model has a radius at this epoch that is about 9% larger than the observed value. Below, we consider ways in which better agreement can be achieved for Saturn.

In earlier calculations of the interior structure of Saturn, investigators also experienced difficulties in fitting the observed dimension with models having a solar composition of elements (DeMarcus, 1958; Hubbard, 1969). Agreement can be achieved if the abundance of helium within a homogeneous interior is significantly increased above the solar value (Hubbard, 1969). However, because of the difficulty in finding a mechanism for increasing the helium-to-hydrogen ratio during planetary formation, the plausibility of such enriched, homogeneous models has been called into question (Podolak and Cameron, 1974). In addition, it might be difficult to understand why very little enrichment has occurred for Jupiter, as indicated by the good match between the observed and predicted radii.

In part, the discrepancy between our calculated and the observed radius of Saturn may be due to errors in the EOS and in part due to the presence of chemical inhomogeneities within the planet. Numerical tests carried out in Paper I for Jupiter indicate that Jupiter's computed radius can change by as much as 9% because of uncertainties in the EOS. Furthermore, the most likely correction to the EOS would result in a more compressible material for the molecular phase near the metallic boundary and a less compressible material in the metallic phase near this boundary. In the case of Saturn such corrections would probably lead to a smaller model radius. Since a larger portion of the interior of Saturn ($\sim$70% by mass) than that of Jupiter ($\sim$20%) lies within a region of density where the EOS is least known, it is conceivable that all of the discrepancy between the computed and observed radii of Saturn is due to uncertainties in the EOS. However, the magnitude of such corrections is somewhat constrained by the desire that the computed radius of Jupiter be no smaller than the observed value.

There are two types of chemical inhomogeneity, whose inclusion may lead to a better fit to the observed radius. First, at the center of Saturn, there may be a dense core composed of rocky material, as advocated by Podolak and Cameron (1974). They also suggested that the envelope of Saturn may be enriched in such volatiles as water vapor. As discussed more fully below, the observed radius of Saturn can be matched with a model that has a solar abundance envelope obeying our present EOS and a central rocky core that contains about 20% of the total mass.

A second type of chemical inhomogeneity that will affect the computed radius occurs when helium becomes immiscible in hydrogen. As shown in Fig. 9, the metallic portion of the homogeneous model first crosses its phase separation curve after about 1.2 billion years. Thus, some separation may be present in current-day Saturn. However, the sign of the change in radius caused by this factor is probably in the wrong direction. To study the sign of this effect, we have compared the compressibility of pure hydrogen with that of a solar mixture of elements. Consider the following "thought" experiment. Take a unit mass of material that is enriched in hydrogen and located near the center of the planet; exchange it with a unit mass of material that is enriched in helium and located further from the center. In general, the expansivity of both materials depends more sensitively on pressure than on temperature. Hence, movement of the first test mass to a lower-pressure environment will cause it to expand slightly, and similarly, the second test mass will contract slightly. If the first test mass expands more than the second one contracts, the planet's radius will increase and vice versa. Calculations of the volume change experienced by unit masses of pure hydrogen and a solar mixture of elements

show that the former always expands more than the latter contracts when they are exchanged along the pressure–temperature structure of the 2-billion-year-old model of Saturn. This result suggests, but does not prove, that allowance for helium immiscibility will only aggravate the discrepancy in radius. If this is true, better models will result only with improved EOS and/or allowance for a silicate core.

Origin of Saturn's Excess Luminosity

As mentioned in the Introduction, Saturn's observed excess luminosity is derived ultimately from gravitational potential energy. This source can be divided into three categories: the present rate of contraction of a homogeneous planet, the loss of internal thermal energy that was built up during an early, rapid-contraction phase, and the gravitational sinking of helium toward the center of the planet because of the partial immiscibility of helium in hydrogen. Figure 4 shows that after 4.5 billion years, the evolutionary track of a homogeneous Jupiter passed quite close to the observed excess luminosity. At the same epoch, the predicted luminosity of a homogeneous Saturn is a factor of 3 smaller than the observed value shown in Fig. 4. However, as explained in the last section, a recalibration of some of the data used to obtain the observed excess luminosity of Saturn leads to a reduction of this value by as much as a factor of 3 and hence leads to a substantially improved agreement between the predicted and observed excess luminosities. For both planets the *calculated* internal heat source at present is due mostly to the loss of internal energy, with a small but significant contribution coming from the present rate of contraction (see Fig. 5). The temperatures within the metallic region of Jupiter for the current epoch lie far above the temperatures at which helium first becomes immiscible in metallic hydrogen. Hence, both the luminosity predictions of the homogeneous model and the temperature structure of current-day Jupiter imply that the most important source of its observed excess luminosity is the loss of internal energy and that the gravitational sinking of helium is not a major energy source. A different situation may hold for Saturn.

Because our Saturn model for the current epoch has a somewhat larger radius than the observed value, factors that lead to a better fit in radius—namely, an improved EOS and/or a silicate core—may also enhance the release of gravitational energy in the past and present. Consequently, an improvement in radius may also result in a somewhat larger predicted excess luminosity.

We next discuss the possible contribution to the internal heat source arising from the gravitational separation of helium from hydrogen in the metallic zone. Since the evolutionary curves of our homogeneous models cross the phase separation boundary of helium in metallic hydrogen after about 1.2 billion years, this factor may be important for Saturn. As mentioned in Section III, immiscibility first occurs at the outer boundary of the metallic zone and gradually moves inward with the passage of time. However, it is not known at present whether mass is efficiently exchanged across the molecular/metallic boundary and therefore whether the helium depletion in the outer portion of the metallic zone is shared by the molecular envelope. Also, it is unclear as to whether the temperatures are cold enough in the molecular envelope for helium separation to occur there, too. As seen below, these uncertainties make it very difficult to assess the importance of helium immiscibility for the internal heat source of Saturn.

We have made some crude estimates of the amount of helium separation required for this source of energy to be a principal contributor to the excess luminosity of Saturn. We first considered a case in which the molecular envelope did not participate in the helium segregation, either by exchanging mass with the metallic core or by under-

going its own phase separation. An estimate of the gravitational release accompanying helium separation in the metallic core was obtained by considering the change in the gravitational energy accompanying the exchange of small parcels of pure helium, located initially near the outer portion of the metallic zone, with pure hydrogen parcels of equall mass, located initially near the center of the metallic zone. We found that even with a complete phase separation in the metallic zone the amount of gravitational energy release was about an order of magnitude less than the amount of energy radiated to space for the last several billion years at the current level of excess luminosity. These two energy values could be made comparable only by having the helium segregation shared by the envelope. Thus, if helium immiscibility is an important source of Saturn's excess luminosity at present, its observable atmosphere should be markedly depleted in helium.

In summary, the loss of internal thermal energy along with a smaller amount of energy derived from the present rate of contraction makes important contributions to the present excess luminosity of Saturn. Some energy will also be obtained from the phase separation of helium, which apparently has been occurring for the last several billion years in the metallic zone. However, for this latter energy source to be a major contributor to the internal heat source requires a segregation of helium throughout the whole planet. Whether separation has occurred on this scale is an open question at present.

Magnetic Field of Saturn

The recent detection of radio bursts from Saturn provides strong circumstantial evidence for the presence of a magnetic field (Brown, 1975). Assuming that the radiation is generated at the cyclotron frequency of an electron, and using the observed spectral characteristics of Jupiter's and Saturn's radio bursts, Brown (1975) estimated that Saturn's magnetic field was about eight times weaker than that of Jupiter. The magnetic field of Jupiter is probably generated by a dynamo effect occurring within the metallic zone of the planet (Hubbard and Smoluchowski, 1973: Smoluchowski, 1975). Within this zone all three conditions needed for a dynamo to operate occur: the presence of a fluid, a high electrical conductivity, and a drive for motions supplied by convective energy transport. These conditions are also met in the metallic zone of Saturn, but not in its essentially unionized molecular envelope.

It is interesting to note that part of the difference in the strength of the magnetic fields for the two planets may be due to a difference in the sizes of their metallic zones. According to Busse's (1975) dynamo theory, for example, the field strength at the surface of a planet scales in the following way with the size of the region in which dynamo action is occurring:

$$H \sim R\ (r_c/R)^3, \tag{2}$$

where r_c is the radius of the dynamo region and R is the planetary radius. As pointed out in Section III, $r_c/R \cong 0.78$ for Jupiter's metallic zone and $r_c/R \cong 0.37$ for Saturn's metallic zone. Thus, solely on the basis of a difference in the sizes of their metallic zones, we expect that the magnetic field of Saturn should be about an order of magnitude weaker than that of Jupiter, an expectation that is consistent with Brown's (1975) results. Naturally, a number of additional factors not considered here also enter into the determination of the magnetic field strength produced by a dynamo.

Consequences of a Silicate Core

Because our homogeneous model of Saturn after 4.5 billion years of evolution differs significantly in radius from the observed value, it is important to assess the impact of improved models on some of our conclusions. As discussed above, one possible way of obtaining an improved model, though by

no means necessarily the only way, is to introduce a rocky core into the center of the planet, Below, we consider such an inhomogeneous model for the current epoch only.

Summers, Reynolds, and Fisher (private communication) have constructed a static model of present-day Saturn that consists of an outer envelope containing a solar mixture of elements and an inner rocky core. The equations of state used in this paper for our homogeneous model were employed for the outer envelope. In contrast to our calculations, allowance for rotational effects was made in constructing the inhomogeneous model. The mass of the silicate core was adjusted until agreement was achieved with the observed radius. Summers *et al.* found that a core mass slightly in excess of 20 Earth masses, i.e., slightly more than 20% of Saturn's mass, was required to meet this condition.

We have used the internal structure of the inhomogeneous model to reexamine some of the conclusions reached above. In accord with our results for the homogeneous model, we find that the entire molecular and metallic hydrogen zones of the planet are in a fluid state; the volume of the metallic zone of Saturn is about an order of magnitude smaller than that of Jupiter; and as a consequence of this volume difference Busse's (1975) dynamo model implies that the magnetic field strength of Saturn should be about an order of magnitude smaller than that of Jupiter. The last inference is in accord with currently available observations, as discussed above.

Finally, the temperatures within the metallic hydrogen zone of the inhomogeneous model are somewhat warmer than those of the homogeneous model. As a result, only a very narrow zone near the molecular/metallic phase boundary lies below the H/He phase separation curve. Hence, little differentiation has occurred up until the current epoch and in this case energy of differentiation is not a major heat source. This comparison suggests that while the temperatures of the interior of present-day Saturn are close to the phase separation curve, an accurate assessment of the amount of separation that has taken place must await the construction of improved models of Saturn as well as improved determinations of the phase separation curve.

Formation of the Satellites and Rings of Saturn

As discussed in the Introduction, the very high luminosity that characterized Jupiter's early contraction history may have inhibited the condensation of water ice in the vicinity of the inner Galilean satellites. This may help to explain why Io and Europa apparently contain much less water ice than do Ganymede and Callisto. Figure 4 shows that during its early contraction phase Saturn also had a high luminosity, but this value was about an order of magnitude smaller than that of Jupiter. Hence, we might expect that Saturn's inner satellites could contain a large amount of water ice, as is implied by their densities (Morrison and Cruikshank, 1974). It is even conceivable that water ice could have condensed in the region of the rings near the end of the satellite formation period. These topics will be treated in greater detail in another paper (Pollack *et al.*, 1976).

V. CONCLUSIONS

Figures 1 to 9 and Table II summarize the results of our calculations of the gravitational contraction history of a homogeneous model of Saturn that contains a solar abundance mixture of elements. The evolutionary tracks are similar to those found by Paper I for Jupiter. Both planets experience an early, rapid contraction phase that is characterized by a buildup of internal thermal energy, high luminosity, and effective temperature, and a later, much longer, slower contraction phase in which the internal temperatures continually decrease along with the luminosity and effec-

tive temperature. However, it is the differences between the evolutionary behavior of the two planets that are most intriguing. These are detailed below.

Our calculations permit some tentative conclusions to be drawn about the state of the matter in the interior of Saturn. A metallic hydrogen zone probably is present near the center of the planet, but the fraction of the planetary mass contained in this zone is almost an order of magnitude smaller than that for Jupiter. The difference in extent of the metallic regions for the two planets may in part be responsible for the difference in the strength of their magnetic fields. The present temperatures in both the molecular and metallic regions of Saturn are far above the freezing point. Thus, the materials in both zones are in a fluid state, as is the case of Jupiter. However, in contrast to Jupiter, the temperature in the outer portion of Saturn's metallic region apparently became cool enough after 1.2 billion years of evolution for helium separation to commence. This would have led to an enrichment of helium in the inner portion of this region and a depletion in the outer portion over Saturn's subsequent 3 billion years of evolution up until the present.

After 4.5 billion years, the calculated values of Jupiter's radius and excess luminosity are consistent with the observed values. However, the Saturn model is somewhat less successful (see Figs. 3 and 4). The computed radius is about 9% larger than the measured value, while the computed luminosity is comparable to the most recent estimates of the excess luminosity. The discrepancy in radius may be corrected by improvements in the EOS and/or allowance for a rocky core. However, a comparison of the compressibility of pure hydrogen with that of a solar mix suggests that helium separation will cause the planet to expand. Improvement in the model radius may also lead to somewhat larger predicted luminosities. The loss of internal thermal energy, built up during Saturn's early rapid contraction, makes an important and perhaps dominant contribution to the present excess luminosity. Saturn's present rate of contraction makes a secondary contribution. These two factors, in a similar proportion, control Jupiter's excess luminosity. However, in the case of Saturn, at least some of the excess luminosity may also be produced by helium segregation. For this to be the dominant factor requires helium separation to occur on a planetwide scale, in which case there should be a noticeable depletion of helium in Saturn's observable atmosphere.

Our present-day homogeneous model was compared with an inhomogeneous model containing a solar mix envelope and a central rocky core. The latter model had a radius equal to the observed value. We found that our conclusions remained unaltered about the fluid state of the molecular and metallic hydrogen zones and the approximate relative strength expected for Jupiter's and Saturn's magnetic fields. However, only a tiny portion of the metallic zone of the inhomogeneous model lay below the H/He phase separation curve. Thus, the amount of helium differentiation and its importance for the internal heat source remains unclear at present.

Saturn's early high luminosity may have influenced the formation of its satellites and rings, as seems to be the case for Jupiter. However, because Saturn's luminosity was about an order of magnitude smaller than Jupiter's during this epoch, water–ice satellites were able to form closer to Saturn.

ACKNOWLEDGMENT

This work was supported in part by the Office of Planetology Programs, NASA.

REFERENCES

AUMANN, H. H., GILLESPIE, C. M., JR., AND LOW, F. J. (1969). The internal powers and effective temperatures of Jupiter and Saturn. *Astrophys. J.* **157**, L69–L72.

BODENHEIMER, P. (1974). Calculations of the early evolution of Jupiter. *Icarus* **23**, 319–325.

BROWN, L. W. (1975). Saturn radio emission near 1 MHz. *Astrophys. J.* **198**, L89–L92.

BUSSE, F. (1975). Generation of planetary magnetism by convection. To be published.

DEMARCUS, W. C. (1958). The constitution of Jupiter and Saturn. *Astron. J.* **63**, 2–28.

FLASAR, F. M. (1973). Gravitational energy sources in Jupiter. *Astrophys. J.* **186**, 1097–1106.

GRABOSKE, H. C., JR., OLNESS, R. J., AND GROSSMAN, A. S. (1975a). Thermodynamics of dense hydrogen–helium fluids. *Astrophys. J.* **199**, 255–264.

GRABOSKE, H. C., JR., POLLACK, J. B., GROSSMAN, A. S., AND OLNESS, R. J. (1975b). The structure and evolution of Jupiter: The fluid contraction stage. *Astrophys. J.* **199**, 265–281. Referred to in text as "Paper I."

GROSSMAN, A. S., AND GRABOSKE, H. C., JR. (1971). Evolution of low mass stars. III. Effects of nonideal thermodynamic properties during the premain sequence contraction. *Astrophys. J.* **164**, 475–490.

GROSSMAN, A. S., GRABOSKE, H. C., JR., POLLACK, J. B., REYNOLDS, R. T., AND SUMMERS, A. (1972). An evolutionary calculation of Jupiter. *Phys. Earth Planet, Interiors* **6**, 91–98.

HOUCK, J. R., POLLACK, J. B., SCHAACK, D., REED, R. A., AND SUMMERS, A. (1975). Jupiter: Its infrared spectrum from 16 to 40 microns. *Science*, to appear. Also Cornell University Report CRSR 594.

HUBBARD, W. B. (1968). Thermal structure of Jupiter. *Astrophys. J.* **152**, 745–754.

HUBBARD, W. B. (1969). Thermal models of Jupiter and Saturn. *Astrophys. J.* **155**, 333–344.

HUBBARD, W. B., AND SMOLUCHOWSKI, R. (1973). Structure of Jupiter and Saturn. *Space Sci. Rev.* **14**, 599–662.

INGERSOLL, A. P., MUNCH, G., NEUGEBAUER, G., DINER, D. J., ORTON, G. S., SCHUPLER, B., SCHROEDER, M., CHASE, S. C., RUIZ, R. D., AND TRAFTON, L. M. (1975). Pioneer 11 infrared radiometer experiment: The global heat balance of Jupiter. *Science* **188**, 472–473.

KIEFFER, H. H. (1967). Calculated physical properties of planets in relation to composition and gravitational layering. *J. Geophys. Res.* **72**, 3179–3197.

KIPPENHAHN, R., WEIGERT, A., AND HOFMEISTER, E. (1967). Methods for calculating stellar evolution. In *Methods in Computational Physics*, Vol. 7, *Astrophysics* (B. Alder, Ed.), pp. 129–190. Academic Press, New York.

MORRISON, D., AND CRUIKSHANK, D. P. (1974). Physical properties of the natural satellites. *Space Sci. Rev.* **15**, 641–740.

NEWBURN, R. L., JR., AND GULKIS, S. (1973). A survey of the outer planets Jupiter, Saturn, Uranus, Neptune, and Pluto, and their satellites. *Space Sci. Rev.* **14**, 179–271.

ORTON, G. S., AND AUMANN, H. H. (1976). Airborne spectroscopic observations of Jupiter between 12 and 25 microns. Presented at the 1976 Annual Meeting of the Division of Planetary Sciences/AAS, Austin, Tex.

PERRI, F., AND CAMERON, A. G. W. (1974). Hydrodynamic instability of the solar nebula in the presence of a planetary core. *Icarus* **22**, 416–425.

PODOLAK, M., AND CAMERON, A. G. W. (1974). Models of the giant planets. *Icarus* **22**, 123–148.

POLLACK, J. B., AND OHRING, G. (1973). A numerical method for determining the temperature structure of planetary atmospheres. *Icarus* **19**, 34–42.

POLLACK, J. B., AND REYNOLDS, R. T. (1974). Implications of Jupiter's early contraction history for the composition of the Galilean satellites. *Icarus* **21**, 248–253.

POLLACK, J. B., GROSSMAN, A. S., MOORE, R., AND GRABOSKE, H. C., JR. (1976). The formation of Saturn's satellites and rings, as influenced by Saturn's contraction history. *Icarus* **29**, 35–48.

RIEKE, G. H. (1975). The thermal radiation of Saturn and its rings. *Icarus* **26**, 37–44.

ROSS, M. (1974). A theoretical analysis of the shock compression experiments of the liquid hydrogen isotopes and a prediction of their metallic transition. *J. Chem. Phys.* **60**, 3634–3644.

ROSS, M., REE, F., AND KEELER, R. N. (1975). A summary of recent work on the equation of state of dense hydrogen. In *Proceedings of the Fourth International Conference on High Pressure Phase Transitions, Kyoto, Japan.*

SALPETER, E. E. (1973). On convection and gravitational layering in Jupiter and in stars of low mass. *Astrophys. J.* **181**, L83–L86.

SMOLUCHOWSKI, R. (1967). Internal structure and energy emission of Jupiter. *Nature (London)* **215**, 691–695.

SMOLUCHOWSKI, R. (1975). Paper presented at the Jupiter Conference, Tucson, Ariz., May 1975; to be published as part of the proceedings of this meeting.

STEVENSON, D. G. (1975). Thermodynamics and phase separation of dense fully-ionized hydrogen–helium fluid mixtures. *Phys. Rev. J.*

WRIGHT, E. L. (1976). Recalibration of the far-infrared brightness temperatures of the planets. Harvard College Observatory Preprint No. 480, submitted to *Astrophys. J.*